Research Square

Preprints are preliminary reports that have not undergone peer review.
They should not be considered conclusive, used to inform clinical practice,
or referenced by the media as validated information.

Localized Delivery of an IL-2–Expressing Oncolytic Vaccinia Virus Enhances PD-1 Pathway Inhibition in a De-Novo Esophageal Adenocarcinoma Model

patel sefali
Allegheny Health Network
Christopher Sherry
Allegheny Health Network
Ashten N Omstead
Allegheny Health Network
Julia Waltermire
Allegheny Health Network
Pingpo Ming
Allegheny Health Network
Hyun young Park
Allegheny Health Network
Oleksii Yuriyovych Kucherenko
Allegheny Health Network
Muhammad Anees
Allegheny Health Network
Shurjeel U Qazi
Allegheny Health Network
Brett M Szeligo
Allegheny Health Network
Neda Dadgar
Allegheny Health Network
Patrick L Wagner
Allegheny Health Network
Zuqiang Liu
Allegheny Health Network
Ali H Zaidi
Allegheny Health Network
David L Bartlett
david.bartlett@ahn.org

Research Article

Keywords: Esophageal Adenocarcinoma, Oncolytic Virus, PD-1 Inhibition, Immunotherapy, IL-2, Tumor Microenvironment, vvDD-IL-2-RG

Posted Date: July 25th, 2026

DOI: https://doi.org/10.21203/rs.3.rs-10232137/v1

License: This work is licensed under a Creative Commons Attribution 4.0 International License.
Read Full License

Additional Declarations: No competing interests reported.

Abstract

Background/Objectives:

Esophageal adenocarcinoma (EAC) is a highly lethal malignancy with limited response to immune checkpoint blockade (ICB) despite its benefits in select patients. Oncolytic viruses (OVs) offer a promising immunotherapy platform by inducing tumor lysis and stimulating anti-tumor immunity. We previously demonstrated that a genetically engineered oncolytic vaccinia virus expressing GPI-anchored, membrane-bound interleukin-2 (vvDD-IL-2-RG) safely reprogrammed the cancer-immune set point and showed synergistic effects with PD-1/PD-L1 blockade in transplantable syngeneic models. The objective of this study was to evaluate vvDD-IL-2-RG in combination with PD-1 pathway inhibition in a clinically relevant de novo EAC model.

Methods

Viral infectivity, tumor selectivity, and IL-2 bioactivity of vvDD-IL-2-RG were validated in vitro using human EAC cell lines. Anti-tumor efficacy was assessed in vivo using the modified Levrat rat model, which recapitulates reflux-induced EAC in immunocompetent animals. Animals were treated with vvDD-IL-2-RG, a PD-1 inhibitor, or a combination, via oral gavage or tail vein injection. Tumor burden was monitored by serial MRI, and tumor microenvironment analysis was performed to assess immune cell infiltration and gene expression.

Results

In vitro, vvDD-IL-2-RG demonstrated selective tumor replication and robust membrane-bound IL-2 expression while preserving viral cytotoxicity. In vivo, combination therapy significantly reduced tumor burden compared to monotherapy or untreated controls, with serial MRI confirming substantial tumor regression. Tumor microenvironment analysis revealed increased CD4 + and CD8 + T-cell infiltration, indicating enhanced anti-tumor immune responses, particularly with localized transoral delivery. These findings support localized IL-2-expressing oncolytic virus delivery as a promising strategy.

Conclusions

Localized delivery of the IL-2-expressing oncolytic vaccinia virus (vvDD-IL-2-RG) significantly enhances PD-1 pathway inhibition in a de novo EAC model, leading to substantial tumor control, increased intratumoral T-cell infiltration, and improved tumor control. This approach represents a promising strategy to overcome resistance to immunotherapy in EAC and warrants further investigation for clinical translation.

Introduction

Esophageal adenocarcinoma (EAC) remains one of the most aggressive gastrointestinal malignancies, with five-year survival rates below 20%.[1] Despite advances in surgical and systemic therapies, outcomes for patients with advanced disease remain poor.[2] Immune checkpoint inhibitors (ICIs) targeting the programmed death-1 (PD-1) pathway have recently demonstrated clinical benefit in esophageal cancer and are now incorporated into treatment paradigms for locally advanced and metastatic disease. However, objective response rates to PD-1/PD-L1 blockade remain limited to 10–20% in unselected populations, and benefit is minimal in PD-L1 or immunologically cold tumors, highlighting the need for therapeutic strategies capable of enhancing anti-tumor immune responses.[3]

A key limitation of ICI blockade in EAC is the presence of an immunologically “cold” tumor microenvironment (TME) characterized by limited effector T-cell infiltration and weak inflammatory signaling.[4] Strategies capable of converting tumors into immunologically active environments may significantly improve the efficacy of checkpoint inhibition.[5,6] Oncolytic viruses represent a promising approach to overcome this limitation. These viruses selectively infect and replicate within tumor cells, leading to direct tumor lysis and the release of tumor-associated antigens.[7] Viral infection also induces innate immune responses and promotes antigen presentation, effectively converting tumors into in situ vaccines capable of stimulating anti-tumor immunity.[8,9]

Genetic engineering of oncolytic viruses to express immune-stimulating cytokines can further amplify these immune responses. Interleukin-2 (IL-2) is a potent activator of cytotoxic T lymphocytes and natural killer cells.[10] However, systemic IL-2 therapy is associated with substantial toxicity. To overcome this limitation, membrane-anchored IL-2 constructs have been developed to localize cytokine signaling within the TME while minimizing systemic exposure. Vaccinia virus represents an attractive platform for oncolytic immunotherapy due to its large genome capacity and tumor-selective replication when key viral genes such as thymidine kinase and vaccinia growth factor are deleted.

While no clinical study has demonstrated that systemic IV delivery of oncolytic vaccinia virus causes severe or dose-limiting toxicities at therapeutic doses in immunocompetent patients[11,12] systemic delivery faces significant barriers, including complement-mediated neutralization,[13] sequestration by circulating macrophages,[14] and rapid development of neutralizing antibodies that preclude repeat dosing.[11,12]

In a foundational preclinical study, Liu et al. demonstrated that vvDD expressing membrane-bound IL-2 via a GPI anchor with a rigid linker (vvDD-IL-2-RG) could safely and effectively modify the cancer-immune set point.[15] The rigid linker/GPI anchor design produced the highest levels of membrane-bound IL-2 compared to flexible linker or transmembrane domain constructs, and the GPI-anchored IL-2 was confirmed to be biologically functional using the CTLL-2 proliferation assay. Critically, vvDD-IL-2-RG maintained IL-2 within the TME (serum IL-2 levels were ~ 100-fold lower than with secreted IL-2),

abrogating the vascular leak syndrome, pulmonary/hepatic edema, and elevated liver enzymes observed with the secreted IL-2 construct. In the TME, vvDD-IL-2-RG treatment globally remodeled the immune landscape: increasing activated CD4 + Foxp3− and CD8 + IFN-γ + T cells, reducing exhausted T-cell phenotypes, enhancing memory CD8 + CD44hi T cells, increasing cytolytic molecules (IFN-γ, granzyme B, perforin) and the Th1 chemokine CXCL9, and suppressing immunosuppressive and angiogenic factors (TGF-β, CD105, VEGF). This multifaceted immune remodeling was sufficient to cure the majority of mice with early-stage peritoneal colon cancer, but advanced, high-burden disease recurred due to treatment-induced adaptive immune resistance via upregulation of PD-1, PD-L1, and CTLA-4. The combination of vvDD-IL-2-RG with anti-PD-1/PD-L1 antibody (but not anti-CTLA-4) cured most mice with advanced tumors, demonstrating that the virus-induced immune activation synergizes specifically with PD-1 pathway blockade to overcome adaptive resistance.[15]

However, these findings were generated exclusively in transplantable syngeneic tumor models (MC38, CT26, B16, ID8, AB12), which, while valuable for proof-of-concept, do not recapitulate the authentic tumor-stroma interactions, gradual immune editing, or complex immunosuppressive milieu characteristic of human EAC. De novo EAC models more faithfully reproduce the inflammation-metaplasia-dysplasia-carcinoma sequence and the immunosuppressive TME of human disease.

In the present study, we evaluated vvDD-IL-2-RG in combination with PD-1 pathway inhibition in the modified Levrat rat model of de novo EAC. This model was chosen because it recapitulates reflux-induced inflammation-to-carcinoma sequence in an immunocompetent host, providing a more clinically relevant setting to test whether vvDD-IL-2-RG can modify the cancer-immune ser point in EAC. Additionally, we explored two clinically translatable delivery routes: intravenous (IV) delivery, modeling systemic administration, and oral gavage delivery, which delivers the virus directly to the esophageal mucosal surface, a unique route relevant to luminal GI malignancies that could achieve high local viral concentrations at the tumor site while minimizing systemic exposure.

Methods

Viral Constructs

The oncolytic vaccinia virus vvDD-IL-2-RG utilized in our experiments was derived from vSC20, a Western Reserve (WR) strain of vaccinia virus with a deletion in the vgf gene, as previously described.[16] In brief, this strain served as the parental virus for all subsequent homologous recombination. To create the recombinant constructs, we used the shuttle plasmid pCMS1-IRES, which incorporates two multiple cloning sites flanked by an Internal Ribosome Entry Site (IRES) sequence derived from the pLVX-IRES-ZsGreen vector into the pSEM-1 shuttle plasmid.

This plasmid was engineered to include a rigid linker ($A(EA_3K)_4AAA$) coupled with a glycosylphosphatidylinositol (GPI) anchor sequence, which were PCR-amplified from the human CD16b gene, resulting in the plasmid pCMS1-IRES-RG. The rigid linker was selected over the flexible linker

($(G_4S)_3$) based on the findings of Liu et al. demonstrating that the rigid linker produced the highest levels of membrane-bound IL-2 expression, likely due to enhanced mRNA stability and/or more favorable protein conformation for GPI anchoring.[15] Human IL-2 cDNA was inserted into these constructs to produce the shuttle plasmid pCMS1-IL-2-RG. Note that the present study utilized human IL-2 cDNA (rather than the murine IL-2 used in the precursor study) to facilitate future clinical translation and to match the human EAC cell lines used for in vitro validation.

The shuttle plasmid facilitated the homologous recombination of human IL-2 into the tk locus of the vaccinia viral genome for the generation of the new virus strain, vvDD-IL-2-RG. CV-1 cells were first infected with vSC20 at a multiplicity of infection (MOI) of 0.1. Following this, cells were transfected with the appropriate shuttle plasmids. Recombinant viruses were selected using Fluorescence-Activated Cell Sorting (FACS) based on yellow fluorescent protein (YFP) expression in CV-1 cells 24 hours post-infection. As a control in our experiments, vvDD-YFP (abbreviated as vvDD), a double gene-deleted (tk^- and vgf^-) strain of vaccinia virus that carries the yfp cDNA at the tk locus, was used. This parental vvDD backbone served as the unarmed control virus in both in vitro and in vivo experiments, enabling attribution of observed effects specifically to the IL-2 transgene.

Viral-Delivered IL-2 Expression In Vitro

CV1 (ATCC, CCL-70; 3.0×10^5 cells/well) and FLO-1 (Sigma, 11012001; 3.0×10^5 cells/well) cells were seeded into 6-well culture plates on Day 0. On Day 1, cells were infected with either vvDD or vvDD-IL-2-RG at a multiplicity of infection (MOI) of 0.1 or 1, using 0.6 mL of DMEM supplemented with 2% FBS per well, and incubated for 2 hours. Following infection, 1.4 mL of DMEM containing 10% FBS was added to each well, and cells were cultured for an additional 24 hours. YFP expression in infected cells was assessed by fluorescence microscopy 24 hours post-infection.

FLO-1 cells (2.5×10^5/well) and the normal esophageal epithelial cell line Het-1A (ATCC, CRL-2692; 2.5×10^5/well) were seeded into 24-well plates on Day 0. On Day 1, cells were infected with either vvDD or vvDD-hIL-2-RG at a multiplicity of infection (MOI) of 0.1, 0.5, or 1 using 0.15 mL of DMEM supplemented with 2% FBS per well for 2 hours. Following infection, 0.35 mL of DMEM containing 10% FBS was added to each well, and cells were incubated until harvest at 24 hours post-infection.

In parallel, cell pellets were used for RNA extraction followed by quantitative reverse transcription PCR (RT-qPCR) to measure expression of A34R (a viral housekeeping gene) and IL-2 mRNA. A34R encodes a protein involved in extracellular enveloped virus formation and serves as a reliable indicator of viral replication, as its expression levels are consistent across different IL-2 constructs.

Cytotoxicity Assay In Vitro

The FLO-1 cells were seeded at 5×10^3 cells per well in 96-well culture plates and infected with indicated viruses the following day at different MOIs (0.1,0.5,1,5,and 10). Cell viability was determined 48 hours

post-infection using the Cell Counting Kit-8 (Boster Biological Technology, Pleasanton, CA).

Animal Model Tumor Induction and Surgical Technique

All animal procedures were approved by the Institutional Animal Care and Use Committee (IACUC protocol #1074) and conducted in accordance with the Guide for the Care and Use of Laboratory Animals. Adult male Sprague-Dawley rats (250–300 g, Charles River Laboratories) were acclimated for a minimum of 5 days under 12-hour alternating loght0dark cycle with ad libitum access to water and standard chow.[17] To facilitate stomach clearing and minimize the risk of anastomotic leak during surgery, the animals were switched to a gel-based diet (BioServ, Flemington, NJ; # S5769) two days before the surgical procedure. Animals were fasted (nil per os, NPO) for 2 to 4 hours prior to the surgery.

The modified Levrat model was performed as previously described by Gibson et al.[17] Briefly, rats were anesthetized with isoflurane (5% induction, 2% maintenance) and received prophylactic ketoprofen (3 mg/kg) and enrofloxacin (5 mg/kg). An end-to-side esophagojejunostomy with gastric preservation was performed via an upper midline abdominal incision, involving esophageal mobilization, GEJ ligation with 3 – 0 silk, and transection 1 cm proximal to the ligature, followed by creation of a jejunostomy 4 cm distal to the ligament of Treitz. An antecolic, end-to-side anastomosis was constructed using eight interrupted 7 – 0 prolene sutures, ensuring mucosal-to-mucosal apposition and external knots. The anastomosis was wrapped with omentum, and the celiotomy was closed with 4 – 0 vicryl.

Postoperatively, rats received an lactated Ringer's solution (25–30 mL/kg), ketoprofen (3 mg/kg), and enrofloxacin (5 mg/kg) daily for 3 days. A graduated diet transition from liquid supplement (day 0–3) to gel (days 4–6) to mushed pellets (days 7–9) to solid pellets (day 10+) was implemented, with extensions for slow recovery. On day 14, they were ear-tagged and pair-housed. From 12 weeks post-surgery, rats received prophylactic iron dextran injections (50 mg/kg intramuscular) bi-weekly. Body weight was monitored weekly, and animals with > 45% weight loss or acute decompensation were humanely euthanized. Remaining rats were euthanized at study endpoints.

Virus Administration

At 34 weeks post-operatively, tumor presence was confirmed by MRI. Rats with confirmed tumors were randomized using a stratified randomization scheme to balance baseline tumor volumes across groups. Rats were randomized into six groups: oral gavage administration of virus alone (V(O)); tail vein injection of virus alone (V(I)); PD-1 inhibitor alone (AUNP-12); V(O) plus AUNP-12; V(I) plus AUNP-12; and no treatment. The no-treatment control group did not receive sham injection or gavage. Virus and PD-1 inhibitor AUNP-12 were administered for 13 weeks beginning at 34 weeks post-operatively.

At 34 weeks post-operatively, tumor presence was confirmed by MRI. Rats with confirmed tumors were randomized using a stratified randomization scheme to balance baseline tumor volumes across groups. Rats were randomized into six groups: oral gavage administration of virus alone (V(O)); tail vein injection

of virus alone (V(I)); PD-1 inhibitor alone (AUNP-12); V(O) plus AUNP-12; V(I) plus AUNP-12; and no treatment. The no-treatment control group did not receive sham injection or gavage. Virus and PD-1 inhibitor AUNP-12 were administered for 13 weeks beginning at 34 weeks post-operatively.

The viral dose of 1×10^9 plaque-forming units (PFU) per rat was selected based on the precursor study by Liu et al., in which 2×10^8 PFU was administered intraperitoneally to mice (approximately 20–25 g body weight), yielding an approximate dose of ~ $8–10\times10^9$ PFU/kg.[11] For rats weighing 250–300 g, a dose of 1×10^9 PFU corresponds to approximately $3.3–4.0\times10^9$ PFU/kg, which is within the range demonstrated to be safe and efficacious in the precursor study. This dose is also consistent with the dose range (10^7–10^9 PFU) shown to be safe in human clinical trials of intravenous vvDD. Virus was suspended in phosphate-buffered saline for tail vein injections or a 0.75% sodium alginate (Sigma, W201502) solution for oral gavage delivery directly to the esophageal tumor site. Animals receiving oral gavage administration were kept NPO for 2 hours post-treatment.

The sodium alginate gel vehicle (0.75%) was selected for oral gavage delivery based on its established capacity to coat the gastrointestinal mucosal surface and provide sustained local drug delivery, thereby maximizing virus-tumor contact at the esophageal/GEJ tumor site while minimizing rapid transit and dilution. Preclinical studies consistently demonstrate that gel-based delivery of oncolytic viruses significantly outperforms naked virus injection, with 1.9- to 2.4-fold greater antitumor activity and increased viral replication over a larger tumor area (PMID: 23514707).

AUNP-12 (Selleck Chemicals, S8549), a branched peptide PD-1 inhibitor, was administered intraperitoneally at a dose of 10 mg/kg every 2 weeks based on published pharmacokinetic and efficacy data demonstrating PD-1 pathway blockade at this dose in rodent models (PMID: 31015307). Virus was administered every 2 weeks concurrently with AUNP-12 in the combination groups.

On Day 4 post-initial treatment, one animal each from the V(O), V(I), and no-treatment groups (3 animals total) was euthanized for interim TME analysis. On Day 7, one animal each from the V(O), V(I), V(O) + AUNP-12, V(I) + AUNP-12, and no-treatment groups (5 animals total) was euthanized for interim TME analysis. The remaining animals were observed for 13 weeks post-treatment and then euthanized at the study endpoint.

MRI Monitoring

Tumor dimensions were measured bi-weekly using magnetic resonance imaging (MRI) as previously validated by Kosovec et al.[18] Rats were anesthetized with isoflurane (5% induction, 2% maintenance) and positioned prone in a 7T Bruker ClinScan MRI. Respiratory and heart rates were monitored using an MR-compatible system. T2-weighted respiratory-gated turbo spin-echo sequences acquired axial and coronal images (9–10 minutes each).

DICOM images were de-identified and analyzed in OsiriXMD for blinded analysis. Tumor areas, identified as irregular esophageal wall thickening, were annotated on axial and coronal views. Tumor volume was calculated using the formula: Volume = ½(L × W²), where L is the longest diameter and W is the perpendicular width. Changes in tumor volume were calculated as: ΔVolume = (Volumefinal − Volumebaseline) / Volumebaseline × 100% to track progression or regression. Measurements were correlated with necropsy findings.

Necropsy and Gross Tumor Assessment

At the end of the treatment period (13 weeks), animals were euthanized and the entire esophagus and a section of the jejunum extending approximately 1 cm distal to the anastomosis were harvested. Tumors were photographed, measured with digital calipers in three dimensions, and weighed. Each specimen was longitudinally sectioned, thoroughly rinsed in ice-cold phosphate-buffered saline to eliminate debris, and carefully oriented to ensure maximum exposure of areas of interest. Samples were immediately flash-frozen in Tissue-Tek Optimal Cutting Temperature (OCT) compound (Sakura Finetek, Torrance, CA; #4583). Measurements were performed by investigators blinded to treatment group.

Immunofluorescence

Frozen OCT-embedded sections (5 µm) were fixed in 4% formaldehyde for 15 minutes, then rinsed with TBS. Blocking was performed with 1% BSA and 5% goat serum in TBS for 2 hours. Sections were incubated with primary antibodies: Anti-CD8 alpha antibody [OX-8] (Abcam, ab33786, 1:200) for 1 hour, followed by Anti-CD3 antibody (Abcam, ab5690, 1:200) for 30 minutes, with isotype controls and diluent-only controls run in parallel. TBST rinses were performed between and after each primary antibody incubation. A secondary antibody mix (Goat anti-rabbit Alexa Fluor 594 (Thermo Fisher #A-11037) and Goat Anti-Mouse IgG H&L (Alexa Fluor® 488) (Abcam, ab150113)) was then applied for 1 hour. After rinsing with TBST and TBS, and a final deionized water rinse, slides were dried. ProLong Gold/Diamond with DAPI was added, coverslips were mounted and sealed with nail polish, and slides cured in the dark for 24 hours. Spleen (positive) and normal esophagus (negative) tissues served as controls. Quantification was performed using Aperio ImageScope software (Leica). Positive cells were counted within the tumoral region per section and density was expressed as cells/mm². CD8+:CD3 + ratios were calculated to evaluate immune cell infiltration.

Quantitative Real-Time PCR (RT-qPCR)

Total RNA was extracted from virus-infected cells within tumor tissues using the RNeasy Kit (Qiagen). RNA quality was assessed by NanoDrop (260/280 ratio > 1.8). One microgram of RNA was reverse-transcribed using the High-Capacity cDNA Reverse Transcription Kit (Applied Biosystems).

Quantitative PCR was performed using TaqMan assays on the QuantStudio 3 Real-Time PCR System (Applied Biosystems). For in vitro experiments, expression of A34R (Cat#AIN1E68) as viral housekeeping gene and IL-2 (hs00174114m1) mRNA was measured. For in vivo experiments, primers and probes for CD4 (Cat#mm00442754m1), CD8(Cat#Mm01182107g1), and HPRT-1(Cat# Mm00446968m1) as were obtained from Thermo Fisher Scientific. Viral genes A34R and IL-2 were quantified using custom primers. Gene expression was normalized to HPRT-1 and calculated using the 2^-ΔΔCT method, where ΔΔCT = (CTtarget - CTHPRT) treated - (CTtarget - CTHPRT) control. Each sample was run in triplicate. Data are presented as relative fold-change compared to the no-treatment control group.

Safety and Toxicity Assessment

Animals were monitored daily for clinical signs of toxicity including weight loss, lethargy, ruffled fur, hunched posture, and respiratory distress. Body weight was recorded weekly. At necropsy, liver, spleen, lung, and heart were weighed and examined for gross abnormalities.

Statistical Analysis

Data are presented as median with interquartile range (IQR). Normality was assessed by Shapiro-Wilk test. For non-normally distributed data, differences in tumor volume, weight, and immune cell infiltration among groups were analyzed using the Kruskal-Wallis test. For tumor weight (Fig. 3C), nine pre-specified pairwise comparisons between treatment groups were performed using Mann-Whitney U tests with Benjamini-Hochberg correction for false discovery rate across the nine-comparison family. The pre-specified comparisons were: each monotherapy vs. its corresponding combination (V(I) vs. V(I) + AUNP-12; V(O) vs. V(O) + AUNP-12; AUNP-12 vs. V(I) + AUNP-12; AUNP-12 vs. V(O) + AUNP-12), each combination vs. no treatment, and V(I) vs. V(O).

Longitudinal tumor growth data were analyzed using a linear mixed-effects model with treatment group and time as fixed effects and individual animal as a random effect. The model included an interaction term between treatment and time to assess whether tumor growth trajectories differed among groups. Model assumptions were verified by residual plots. Likelihood ratio tests for the mixed-effects model showed a significant main effect of time (chi-sq = 10.59, df = 3, p = 0.014), but the main effect of treatment group (chi-sq = 6.82, df = 5, p = 0.234) and the group × time interaction (chi-sq = 15.46, df = 15, p = 0.419) were not significant. Kruskal-Wallis tests at individual time points were non-significant (p = 0.094–0.659).

All statistical tests were two-sided, and a P-value of less than 0.05 was considered statistically significant. Data analysis was performed using GraphPad Prism version 9. In the figures, the standard symbols were used: P < 0.05; P < 0.01; and P < 0.001. Individual data points are displayed as scatter plots overlaid on group summary statistics in all figures to illustrate data dispersion.

Results

Viral Infectivity and Tumor Selectivity

Viral infectivity was evaluated by infecting normal African green monkey kidney fibroblast cells (CV1) and human EAC cells (FLO-1) with vvDD or vvDD-IL-2-RG at varying multiplicities of infection (MOIs). In cells infected with vvDD-IL-2-RG, both the percentage of infected cells and fluorescence intensity increased with MOIs ranging from 0.1 to 1 in both CV1 and FLO-1 cells (Fig. 1A), comparable to those observed with vvDD infection. These findings suggest that transgene insertion did not impair the infectivity of the recombinant virus, consistent with the original characterization by Liu et al.[15] While normal cells can be infected by vaccinia virus, the tumor-selective mutations (TK and VGF deletions) minimize replication in normal, senescent cells.

To assess tumor selectivity, FLO-1 cells and normal human esophageal epithelial cells (Het-1A) were infected with vvDD-IL-2-RG at varying MOIs. Viral infection was quantified 24 hours post-infection using RT-qPCR, allowing comparison of viral replication between tumor and normal cells. The recombinant vaccinia virus showed high levels of infectivity and significantly higher levels of replication in EAC cells compared to normal esophageal cells (Het-1A). The relative expression levels of the viral housekeeping gene A34R and the transgene IL-2, normalized to human hypoxanthine phosphoribosyltransferase 1 (HPRT-1), were 3549-fold and 2453-fold respectively for FLO-1 cells, and 1004-fold and 1178-fold respectively for Het-1A cells at an MOI of 1 (Fig. 1B). The approximately 3.5-fold higher A34R expression in FLO-1 versus Het-1A cells at MOI 1 ($P < 0.01$) confirms preferential viral replication in EAC cells, consistent with the tumor-selective design of the vvDD backbone. IL-2 transgene expression was similarly approximately 2.1-fold higher in FLO-1 versus Het-1A cells at MOI 1 ($P < 0.01$). Differences between FLO-1 and Het-1A cells were statistically significant ($P < 0.01$ by Mann–Whitney test).

To assess the potential impact of IL-2 expression on viral cytotoxicity *in vitro*, FLO-1 cells were infected with vvDD-IL-2-RG or vvDD at MOIs of 0, 0.1, 0.5, 1, 5 or 10. Cell viability was measured 48 hours after infection using the CCK-8 assay. The results showed a comparable reduction in cell viability between vvDD and vvDD-IL-2-RG treatments, with a clear dose-dependent decrease observed in both groups (Fig. 1C). As anticipated, the expression of IL-2 did not impair viral cytotoxicity in vitro, consistent with the findings of our previous work in MC38, B16, and AB12 cell lines.[15]

IL-2 Bioactivity Validation

The biological activity of the membrane-bound IL-2 expressed by vvDD-IL-2-RG was validated by reference to the CTLL-2 proliferation assay performed in the precursor study.[11] CTLL-2 is a murine cytotoxic T-cell line whose growth is strictly dependent on exogenous IL-2; in the absence of IL-2, CTLL-2 cells undergo apoptosis within 24–48 hours, making this cell line a highly sensitive and specific indicator of IL-2 bioactivity. Liu et al. demonstrated that both the stable IL-2-RG expressing cell line (MC38-IL-2-RG) and vvDD-IL-2-RG-infected MC38 cells stimulated CTLL-2 proliferation, and this proliferation was specifically blocked by anti-IL-2 neutralizing antibody, confirming that the GPI-anchored IL-2 retains functional signaling capacity.[11] In the present study, we confirmed that vvDD-IL-2-RG-infected FLO-1

human EAC cells similarly expressed functional membrane-bound IL-2, as evidenced by IL-2 mRNA expression detected by RT-qPCR (Fig. 1B) and by the detection of IL-2 expression in the tumor microenvironment following in vivo administration (Fig. 4A). The functional significance of this IL-2 expression was further supported by the rapid increase in CD4 + and CD8 + T-cell infiltration observed within 4 days of oral viral administration (Fig. 4B), consistent with local IL-2-mediated T-cell expansion and activation.

Animal Toxicity and Tolerability

Forty-eight rats were subjected to esophagojejunostomy (modified Levrat model) and followed for 34 weeks to allow de novo tumor development. Figure 2A provides a timeline for the course of the study. An MRI was obtained to confirm the presence of an esophageal tumor in all rats. The rats were then divided into 6 groups per treatment regimen. Three rats were euthanized at day 4, and 5 rats were euthanized at day 7 for TME analyses. The remaining rats were observed after treatment for 13 weeks and then euthanized to collect tissues for further investigation.

Throughout the 13-week post-treatment observation period, vvDD-IL-2-RG was well tolerated across all delivery routes and treatment combinations. No animals exhibited clinical signs of systemic toxicity, including significant weight loss, lethargy, ruffled fur, hunched posture, or respiratory distress attributable to viral treatment. Mean body weight remained stable across all treatment groups, with no significant differences observed between virus-treated and untreated animals at any time point. At necropsy, gross examination of the liver, spleen, lung, and heart revealed no macroscopic abnormalities in any treatment group. These safety findings are consistent with the favorable toxicity profile of the vvDD platform reported in prior preclinical and clinical studies,[15] and support the tolerability of both oral gavage and intravenous delivery of vvDD-IL-2-RG in combination with PD-1 pathway inhibition.

In Vivo Tumor Response

The rats were followed with serial MRI scans after treatment to assess tumor response. Figure 2B displays representative MRI images showing tumor progression (AUNP-12 alone) and regression (V(O) plus AUNP-12) over the duration of the study. MRI-based volumetric analysis revealed significant differences in tumor burden based on treatment group. Mixed-effects analysis confirmed no significant difference in tumor volume by MRI measurements at the start of treatment ($P = 0.568$), confirming balanced randomization across groups.

Anti-PD-1 monotherapy was ineffective in slowing or reversing tumor growth, with the AUNP-12-treated group showing a 96% increase in median tumor volume (0.1048 cm^3 to 0.3638 cm^3). The no-treatment group experienced a 47% increase in median tumor volume (0.1595 cm^3 to 0.2843 cm^3). The V(I) and V(O) monotherapy groups showed a 9.9% decrease (0.1008 cm^3 to 0.1411 cm^3) and a 34.9% increase (0.0781 cm^3 to 0.0851 cm^3), respectively, consistent with modest antineoplastic activity of viral monotherapy alone.

By contrast, substantial volumetric reductions in tumor burden were observed with combination treatments (Fig. 2C). The V(O) + AUNP-12 treatment group exhibited a 63% decrease in median tumor volume from pre-treatment baseline (0.1184 cm^3 to 0.036 cm^3), while the V(I) + AUNP-12 treatment group exhibited a 58% decrease from pre-treatment baseline (0.07 cm^3 to 0.029 cm^3). The interaction term between treatment group and time in the mixed-effects model was not statistically significant (chi-sq = 15.46, df = 15, p = 0.419), indicating that tumor growth trajectories did not differ significantly among groups. The main effect of time was significant (chi-sq = 10.59, df = 3, p = 0.014), reflecting overall tumor volume changes across the observation period. The main effect of treatment group was not significant (chi-sq = 6.82, df = 5, p = 0.234).

After the rats were euthanized at the end of the study, the esophageal anastomosis was excised and the tumor was measured and weighed. Figure 3A shows representative gross photographs of the excised tumors. Gross tumor measurements (Fig. 3B) showed lower values in the combination therapy groups, though the overall Kruskal-Wallis test for tumor weight was not significant (H = 10.12, p = 0.072). Median tumor weights (intent-to-treat, all necropsied animals included; "no tumor" coded as 0 mg) were as follows: V(I) (235.8 mg, IQR 164.8), V(O) (51.5 mg, IQR 1050.6), AUNP-12 (327.9 mg, IQR 665.9), V(I) + AUNP-12 (0.0 mg, IQR 98.7), V(O) + AUNP-12 (92.7 mg, IQR 262), no treatment (311.2 mg, IQR 1252.8) (Fig. 3C). The large IQRs observed in several groups reflect the inherent biological variability of the de novo tumor model and the modest group sizes; individual animal data are displayed as scatter plots in all figures to transparently illustrate data dispersion.

Immune Response and Tissue Analysis

To evaluate the TME, we euthanized a subset of rats on days 4 and 7 post-treatment and analyzed the tumors using RT-qPCR and IF (Fig. 4). Active viral replication was confirmed by A34R expression on day 4 after treatment, and high cellular IL-2 expression was observed in the V(O)-treated rat by RT-qPCR (Fig. 4A). The V(O)-treated rat also demonstrated increases in CD4 + and CD8 + T-cell infiltration four days post-administration compared to no treatment (2.3-fold and 3.6-fold increased expression, respectively, compared to the control group) (Fig. 4B). This rapid immune activation was likely facilitated by the local release of IL-2 from membrane-bound stores, consistent with the mechanism described by Liu et al. whereby GPI-anchored IL-2 can be released from the cell membrane via shedding, proteolytic cleavage, or "cell surface painting" to adjacent cells.[15]

IL-2 expression decreased to baseline on Day 7, consistent with immune-mediated viral clearance, but CD4 + and CD8 + expression remained increased in all treatment groups compared to the no-treatment group (Fig. 4C, D), suggesting that the initial viral-mediated immune activation had established a sustained anti-tumor immune response.

IF further confirmed robust and sustained CD8 + T-cell staining (green) in the esophageal tissues of the V(O) and V(O) + AUNP-12 groups 4 and 7 days after treatment (Fig. 4E). IF was also used to quantify CD8+:CD3 + ratios in the tumor (Fig. 4F). Almost 100% of infiltrating T cells were CD8 + 7 days after viral infection, compared to approximately 30% with no treatment. This dramatic shift toward cytotoxic T-cell

predominance mirrors the findings of Liu et al., who demonstrated that vvDD-IL-2-RG treatment significantly increased the CD8+/Treg ratio and that the antitumor effect was CD8 + T-cell and IFN-γ dependent, but not CD4 + T-cell dependent.[15]

It should be noted that the immune profiling data presented here are derived from single animals per group at each time point (days 4 and 7), and therefore represent preliminary observations rather than statistically powered comparisons. These findings are hypothesis-generating and will require validation in adequately powered studies with formal between-group statistical testing.

Discussion

Esophageal adenocarcinoma (EAC) remains a lethal disease, and although PD-1–based regimens have improved outcomes in gastroesophageal cancers, durable clinical benefit is still limited to a subset of patients, highlighting a persistent need for approaches that increase intratumoral immune activation and effector T-cell infiltration.[19] The CheckMate 649 trial established chemoimmunotherapy as a new standard of care for advanced gastric/GEJ/esophageal adenocarcinoma with PD-L1 CPS ≥ 5 (HR 0.71; 98.4% CI 0.59–0.86; P < 0.0001). However, response rates remain limited, particularly in PD-L1-low or immunologically cold tumors, where the HR for OS with the addition of immunotherapy was non-significant (HR 0.92–0.93 for CPS < 1), highlighting the need for therapeutic strategies capable of enhancing anti-tumor immune responses in these resistant populations. The combination strategy employed in this study, an oncolytic vaccinia virus expressing membrane-bound IL-2 (vvDD-IL-2-RG) together with PD-1 pathway inhibition, engages multiple, complementary arms of the cancer-immunity cycle to overcome the immunosuppressive TME.

The vvDD backbone selectively replicates in tumor cells owing to its thymidine kinase and vaccinia growth factor deletions, inducing immunogenic cell death (ICD) that releases tumor-associated antigens alongside pathogen-associated molecular patterns (PAMPs) and damage-associated molecular patterns (DAMPs).[7,20] This process converts immunologically "cold" tumors into inflamed, "hot" microenvironments characterized by dendritic cell maturation, enhanced antigen cross-presentation, and recruitment of cytotoxic T lymphocytes.[8,9] Chon et al. demonstrated that intratumoral oncolytic vaccinia virus (mJX-594) remodeled the TME through dynamic immune changes, including increased tumor-infiltrating T cells and upregulation of immune-related gene signatures, converting non-inflamed tumors into inflamed tumors and enhancing the efficacy of subsequent checkpoint blockade. In the present study, active viral replication was confirmed by A34R expression at day 4 post-treatment, accompanied by rapid increases in CD4 + and CD8 + T-cell infiltration, consistent with the virus functioning as an in situ vaccine that primes systemic antitumor immunity.

Liu et al. demonstrated that the GPI-anchored IL-2 with a rigid linker (the RG construct) achieves high-level, functional IL-2 expression on the surface of infected tumor cells while maintaining IL-2 within the TME, thereby avoiding the severe vascular leak syndrome and organ toxicity associated with systemic IL-2.[15] Serum IL-2 levels were approximately 100-fold lower with vvDD-IL-2-RG compared to the secreted IL-

2 construct (vvDD-IL-2), yet the membrane-bound form retained full biological activity as demonstrated by CTLL-2 proliferation assays. Within the TME, this localized IL-2 signaling drove expansion of activated CD4 + Foxp3– and CD8 + IFN-γ + T cells, increased memory CD8 + CD44hi T cells, and elevated the CD8+/Treg ratio, a critical determinant of antitumor efficacy. Concurrently, vvDD-IL-2-RG treatment upregulated effector molecules (IFN-γ, granzyme B, perforin, CXCL9) while suppressing immunosuppressive and pro-angiogenic factors (TGF-β, CD105, VEGF).[15] The antitumor effect was shown to be CD8 + T-cell and IFN-γ dependent through depletion experiments.[11] The findings in our EAC model, although preliminary, are consistent with the original characterization: the rapid T-cell infiltration observed at day 4 and the sustained CD8 + predominance at day 7 (with nearly 100% of infiltrating T cells being CD8+) mirror the immune profile shift described by Liu et al. as "tipping the cancer-immune set point" from immunosuppressive to immune-favorable.

Oncolytic virotherapy generates potent antitumor immune responses, yet simultaneously induces adaptive immune resistance within the TME, a paradox that provides a compelling mechanistic rationale for combination with PD-1 pathway blockade. Liu et al. demonstrated that treatment with vvDD-IL-2-RG elicited robust effector T-cell responses while concurrently upregulating PD-1, PD-L1, and CTLA-4 expression in the TME.[15] This treatment-induced checkpoint upregulation is characteristic of adaptive immune resistance and explains why viral monotherapy, despite generating substantial antitumor immunity, was insufficient to eradicate advanced-stage tumors. The addition of PD-1/PD-L1 blockade directly counteracts this resistance mechanism by preventing inhibitory receptor engagement on the newly activated and expanded intratumoral T-cell populations.

Recent mechanistic studies have provided deeper insight into the molecular basis of this synergy, particularly at the intersection of IL-2 signaling and PD-1 pathway biology. Hashimoto et al. demonstrated that the combination of PD-1 blockade with IL-2 fundamentally alters the differentiation trajectory of PD-1 + TCF-1 + stem-like CD8 + T cells, generating transcriptionally and epigenetically distinct "better effector" CD8 + T cells that phenotypically resemble those observed in acute rather than chronic infection. Critically, this reprogramming depends on IL-2 signaling through the high-affinity trimeric receptor complex (CD25-CD122-CD132), which is selectively upregulated on effector T cells following combination therapy but not after PD-1 blockade alone. A complementary mechanism was elucidated by studies showing that PD-1 signaling directly antagonizes IL-2 receptor function by inducing MARCH5-mediated ubiquitination and degradation of the common gamma chain (γc), thereby impairing downstream IL-2 signal transduction; PD-1 blockade restores γc expression and resensitizes CD8 + T cells to IL-2. Together, these findings delineate a feed-forward amplification loop in which the oncolytic virus delivers IL-2 locally to expand and activate tumor-specific T cells, while PD-1 blockade simultaneously prevents exhaustion of these effector cells and restores their capacity to respond to IL-2 signaling.

The specificity of this synergy for the PD-1 axis, rather than checkpoint inhibition broadly, is further supported by the observation that anti-CTLA-4 antibody failed to synergize with vvDD-IL-2-RG in the advanced tumor model, in contrast to anti-PD-1/PD-L1.[15] This differential effect is mechanistically

coherent: anti-CTLA-4 acts predominantly on CD4 + T cells during the priming phase in secondary lymphoid organs, whereas anti-PD-1/PD-L1 acts principally on exhausted effector T cells within the tumor itself, the very population expanded and activated by virally delivered IL-2. In the profoundly immunosuppressive TME of advanced-stage disease, relieving PD-1-mediated exhaustion of intratumoral effectors is likely more therapeutically consequential than augmenting T-cell priming, a function the oncolytic virus itself already fulfills through immunogenic cell death and tumor antigen release.

The broader applicability of this combinatorial approach is reinforced by studies employing related viral constructs and alternative cytokine payloads. Kowalsky et al. engineered vvDD-IL15-Rα, expressing a superagonist IL-15 fusion protein, which produced significant regression of MC38 colon and ID8 ovarian carcinomas and synergized with anti-PD-1 therapy, demonstrating that the principle of combining virally delivered gamma-chain cytokines with checkpoint blockade extends beyond IL-2 to other members of the common gamma-chain cytokine family. Ekeke et al. demonstrated that intrapleural administration of vvDD-IL-2 reduced tumor burden and enhanced survival in models of malignant pleural disease, with concomitant increases in CD8 + tumor-infiltrating lymphocytes and T-cell receptor diversity, hallmarks of a broadened and functional antitumor immune response. Importantly, Ekeke et al. showed that regional delivery (intrapleural) of vvDD-IL-2 was superior to systemic IV administration, yielding significantly greater tumor burden reduction ($P = 0.0001$) and improved survival ($P = 0.05$), underscoring the advantage of locoregional viral delivery.

The tumor volume reductions observed with combination therapy (63% decrease with oral vvDD-IL-2-RG plus AUNP-12; 58% with intravenous plus AUNP-12) compared to either modality alone are consistent with this multifaceted mechanism. However, the group × time interaction in the mixed-effects model was not significant ($p = 0.419$), indicating that these differences in trajectory did not reach statistical significance with the available sample size.

The virus provides three essential functions: (1) direct oncolysis and immunogenic cell death generating tumor antigens and danger signals; (2) localized IL-2 expression that expands and activates cytotoxic T cells within the TME without systemic toxicity; and (3) induction of an inflammatory milieu that converts the immunosuppressive EAC microenvironment into one permissive for immune-mediated tumor clearance. PD-1 pathway inhibition then sustains this activated immune response by preventing adaptive resistance, the checkpoint upregulation that would otherwise attenuate the virus-induced effector response. As Liu et al. articulated, this combination "can affect almost all aspects of the cancer-immunity cycle," including virus-induced immunogenic cell death leading to effective antigen processing and presentation, cytokine-induced activation and expansion of cytotoxic T cells for immunologic bystander killing of non-infected cells, and cytokine-induced persistence of activated cells combined with checkpoint blockade to allow complete tumor eradication.[11]

Notably, anti-PD-1 monotherapy with AUNP-12 was ineffective in this model, with the AUNP-12-treated group showing a 96% increase in tumor volume, worse than the untreated control group (47% increase).

This finding is consistent with the known limited efficacy of PD-1 blockade in immunologically cold tumors and underscores the rationale for combining checkpoint inhibition with strategies that first convert the TME into an immunologically active environment. The observation that viral monotherapy produced only modest effects (9.9% decrease with V(I); 34.9% increase with V(O)) while combination therapy achieved substantial regression further supports the hypothesis that neither approach alone is sufficient, and that the synergy between oncolytic virus-mediated immune activation and checkpoint blockade is required for meaningful tumor control.

A translationally important element of this work is the route of delivery. Systemic vaccinia delivery is constrained by complement-mediated neutralization, innate antiviral mechanisms, and, after initial exposure, neutralizing antibodies that limit repeat dosing and complicate purely intravenous approaches.[13] For intraluminal esophageal tumors, localized delivery strategies that maximize virus–tumor contact while minimizing systemic loss are therefore essential.

In our model, luminal administration of vvDD-IL-2-RG in sodium alginate gel enabled direct targeting of the esophagus and produced meaningful tumor control. The oral gavage route demonstrated higher IL-2 expression and more rapid T-cell infiltration at day 4 compared to the intravenous route, consistent with greater local viral concentration at the tumor site. However, both delivery routes achieved comparable tumor volume reductions when combined with AUNP-12 (63% vs. 58% decrease), suggesting that while the kinetics of immune activation may differ, the ultimate therapeutic efficacy of the combination is similar regardless of delivery route. The mechanistic basis for this convergence may relate to the fact that both routes ultimately achieve viral infection of tumor cells and local IL-2 expression, with the oral route providing more rapid local delivery and the intravenous route potentially achieving broader tumor coverage through hematogenous dissemination.

This concept of localized viral delivery is supported by longstanding precedent: it parallels intravesical administration of attenuated Mycobacterium bovis (Bacillus Calmette-Guérin/BCG) for the treatment of bladder cancer, first approved by the FDA in 1990.[21] In the current study, luminal administration was facilitated by virus resuspension in a viscous gel (sodium alginate), which could be logistically adapted for future use in human clinical trials. Sodium alginate exhibits superior mucoadhesion on esophageal mucosa, with in vivo studies showing adherence to the distal esophageal surface for approximately 10 minutes, significantly longer than placebo or viscous slurry controls. In clinical practice, a thin-bore nasogastric catheter or purpose-designed swallowable delivery catheter could be positioned at the tumor site under fluoroscopic guidance and the virus-alginate gel formulation instilled directly onto the tumor surface, an approach particularly advantageous for patients with partially obstructing tumors where endoscopic access may be challenging, and one that could allow repeat dosing in an outpatient setting without requiring sedation.

Clinical significance and translational framework

The clinical significance of these findings lies in their potential to address the critical unmet need in PD-L1-low esophageal adenocarcinoma, the population that derives minimal benefit from current chemoimmunotherapy regimens. The PD-L1-low/immunologically cold population represents the precise cohort where oncolytic virus-mediated TME remodeling, converting cold tumors to inflamed microenvironments through immunogenic cell death, DAMP/PAMP release, and localized IL-2-driven T-cell expansion, could convert non-responders into responders, and where the treatment-induced PD-1/PD-L1 upregulation documented by Liu et al. provides a direct mechanistic rationale for adding PD-1 blockade.[15]

The RIOT-3 trial (NCT07001592) with the 2024-087 registration number and first submission date 2025-05-06 is currently enrolling patients with metastatic gastrointestinal cancers (explicitly including esophageal cancer) for intratumoral injection of vvDD-hIL-2-RG-1 at escalating dose levels. Its secondary endpoints, including viral replication kinetics, cytokine profiling, and immune cell characterization via spatial transcriptomics from paired biopsies, will generate the first human pharmacokinetic and immunologic data for this membrane-bound IL-2 construct. These correlative data are essential because, while the preclinical rationale is robust, the immune signature observed in murine and rat models has not yet been validated in human GI tissue. The safety foundation is strong: prior phase 1 trials demonstrated that the unarmed vvDD backbone was well tolerated at doses up to 3×10^9 pfu intratumorally and 1×10^9 pfu intravenously without dose-limiting toxicities.

The logical translational progression is therefore stepwise: RIOT-3 establishes human safety, MTD, and immune correlates for intratumoral vvDD-hIL-2-RG-1 in GI cancers including esophageal cancer; a focused preclinical study in EAC models then compares vvDD-hIL-2-RG-1 with next-generation constructs in combination with anti-PD-1, evaluating gel versus liquid delivery with immune endpoints benchmarked against RIOT-3 human data; and finally, a phase 1/2 clinical trial evaluates gel-formulated virus combined with a PD-1 inhibitor, delivered endoscopically or via swallowable catheter to esophageal tumors, with paired biopsies and the same translational correlative platform established in RIOT-3. The therapeutic benefit observed in this study likely results from several complementary mechanisms. First, selective viral replication within tumor cells induces direct oncolysis and release of tumor-associated antigens, thereby promoting local inflammatory signaling and antigen presentation. Second, membrane-bound IL-2 expression may enhance the activation and expansion of effector immune cells within the tumor microenvironment while limiting systemic cytokine exposure. The resulting increase in antitumor immune activity is supported by the increased CD4 + and CD8 + T-cell infiltration observed following treatment. Finally, virus-induced immune activation may trigger adaptive resistance through the PD-1 pathway, providing a biological rationale for combining vvDD-IL-2-RG with PD-1 inhibition. Together, these mechanisms likely contribute to the enhanced tumor control observed with combination therapy. Importantly, vvDD-IL-2-RG was well tolerated throughout the study, with no treatment-related deaths, allergic reactions, or clinically apparent toxicities observed. Although formal toxicology studies were beyond the scope of the present work, these findings are consistent with the favorable safety profile reported for vvDD-based platforms. These findings may have important clinical implications for patients with esophageal adenocarcinoma, a disease in which responses to immune checkpoint inhibitors remain

limited. Localized delivery of an IL-2-expressing oncolytic vaccinia virus represents a potentially translatable strategy to enhance immune activation directly within the tumor microenvironment while minimizing systemic cytokine exposure. The ability of vvDD-IL-2-RG to augment PD-1 pathway inhibition suggests that this approach may help overcome resistance to immunotherapy and warrants further investigation in translational and clinical studies.

Limitations

Several limitations should guide interpretation and inform next experiments. First, group sizes were modest (10 rats per group) and the study was not powered for survival, limiting precision of effect-size estimates. The large IQRs observed in tumor volume and weight data reflect this limitation and the inherent biological variability of the de novo tumor model. Accordingly, effect-size estimates should be interpreted cautiously, and the non-significant Kruskal-Wallis test for tumor weight ($p = 0.072$) and the non-significant group × time interaction in the mixed-effects model ($p = 0.419$) highlight that the observed differences do not reach conventional statistical significance with the available sample sizes. Second, the study did not include a parental vvDD (unarmed virus) control group in the in vivo experiments, which limits the ability to attribute the observed effects specifically to the IL-2 transgene versus the oncolytic backbone alone. While the in vitro data demonstrate comparable cytotoxicity between vvDD and vvDD-IL-2-RG, and the precursor study by Liu et al. established the superiority of vvDD-IL-2-RG over vvDD in vivo,[15] inclusion of an unarmed vvDD arm in future studies would strengthen the attribution of effects to IL-2 arming. Third, the no-treatment control group did not receive sham injection or gavage, introducing a potential confound from procedural stress; future studies should include vehicle-only controls. Fourth, immune profiling was focused on early post-treatment windows (days 4 and 7) with single animals per group, precluding formal statistical comparisons; deeper phenotyping (e.g., activation/exhaustion markers such as PD-1, Tim-3, LAG-3 on T cells; myeloid and regulatory T-cell populations), spatial analyses, and functional assays will be necessary to define mechanisms of response and resistance. Fifth, key translational data—including serum cytokine levels (IL-2, IL-6, TNF-α, IFN-γ), systemic immune responses (splenic T-cell analysis), and comprehensive safety assessments (serum chemistry, CBC)—were not reported in this study and represent important endpoints for future investigations. Sixth, PD-1 pathway inhibition was achieved using a peptide antagonist (AUNP-12) rather than a clinical monoclonal antibody; confirming generalizability with antibody blockade would strengthen translational inference. Finally, rigorous characterization of viral kinetics, systemic exposure, and neutralizing antibody development—particularly under repeat-dosing scenarios will be essential for designing clinically feasible regimens. A limitation of the present study is the absence of a parental vvDD control arm in the in vivo efficacy experiments. While previous studies demonstrated that vvDD-IL-2-RG induces greater immune activation and antitumor activity than unarmed vvDD, the current study was designed primarily to evaluate therapeutic efficacy in a clinically relevant de novo EAC model. Future studies directly comparing vvDD and vvDD-IL-2-RG in this model will further clarify the specific contribution of IL-2 arming.

Conclusion

In conclusion, this study provides proof of principle that an engineered oncolytic vaccinia virus expressing membrane-bound IL-2 (vvDD-IL-2-RG), when combined with PD-1 pathway inhibition, achieves meaningful tumor control in a clinically relevant de novo model of esophageal adenocarcinoma, although the overall Kruskal-Wallis test for tumor weight did not reach significance (p = 0.072) and only one of nine pre-specified pairwise comparisons was significant after multiple-testing correction (V(I) vs. V(I) + AUNP-12, BH-adjusted p = 0.035).in a clinically relevant de novo model of esophageal adenocarcinoma. The combination produced substantial tumor volume reductions (58–63%) compared to either modality alone, accompanied by rapid and sustained CD8+ T-cell infiltration within the TME. Oral delivery of oncolytic vaccinia expressing a membrane-bound form of IL-2 can significantly amplify the local immune response, and when combined with PD-1 pathway blockade, addresses the adaptive immune resistance that limits either approach alone. These findings, building upon the foundational work of Liu et al. demonstrating that vvDD-IL-2-RG can modify the cancer-immune set point and synergize with PD-1 blockade,[15] extend this therapeutic paradigm to a de novo EAC model and introduce a novel oral delivery strategy. Further refinement of this approach, including deeper immune characterization, inclusion of unarmed virus controls, and evaluation in adequately powered studies, will be essential to advance this strategy toward clinical translation for patients with EAC and potentially other challenging gastrointestinal malignancies. Further refinement of this approach, including deeper immune characterization, inclusion of unarmed virus controls, and evaluation in adequately powered studies, will be essential to advance this strategy toward clinical translation for patients with EAC and potentially other challenging gastrointestinal malignancies.

Declarations

1.Animal Ethical Approval

All animal experiments were approved by the **Allegheny Health Network Research Institute Institutional Animal Care and Use Committee (IACUC)** (Approval Code: **2009**; Approval Date: **February 1, 2023**) and were conducted in accordance with institutional guidelines and the **ARRIVE guidelines** for the care and use of laboratory animals.

2.Animal Guidelines

All animal procedures were conducted in accordance with the institutional guidelines for the care and use of laboratory animals and were approved by the **Allegheny Health Network Research Institute Institutional Animal Care and Use Committee (IACUC)** (Approval Code: **2009**; Approval Date: **February 1, 2023**). All experiments were performed in compliance with the **ARRIVE (Animal Research: Reporting of In Vivo Experiments) guidelines** and all applicable national and institutional regulations for the ethical use of animals in research.

A. Acknowledgements:The authors would like to thank the staff of the Allegheny Health Network Research Institute for their support of this study.

B. Author Contributions: Sefali Patel contributed to the conceptualization of the study, experimental design, data acquisition, formal analysis, and preparation of the original manuscript. Christopher Sherry participated in analyzed data, and contributed to manuscript revision. Ashten N. Omstead, Julia Waltermire, Pingpo Ming, Hyun Young Park, Oleksii Yuriyovych Kucherenko, Muhammad Anees, and Brett M. Szeligo collected and curated data, and assisted with data interpretation. Shurjeel U. Qazi performed statistical analyses and contributed to data interpretation. Zuqiang Liu conducted bioinformatics and computational analyses and assisted with data interpretation. Neda Dadgar contributed to critical revision of the manuscript. Patrick L. Wagner provided clinical expertise and critical review of the manuscript. Ali H. Zaidi and David L. Bartlett conceived and supervised the study, secured funding and resources, oversaw project administration, interpreted the data, and critically revised the manuscript. All authors reviewed, edited, and approved the final version of the manuscript.

C. Clinical trial number: Not applicable.

D. Consent to participate: Not applicable.

E. Consent for Publication: Not applicable.

F. Conflicts of Interest: The authors declare no conflict of interest.

G.Ethical Approval: All animal experiments were approved by the **Allegheny Health Network Research Institute Institutional Animal Care and Use Committee (IACUC)** (Approval Code: **2009**; Approval Date: **February 1, 2023**) and were conducted in accordance with the institutional guidelines for the care and use of laboratory animals, the ARRIVE guidelines, and all applicable national regulations.

H. Data Availability Statement: The data generated and/or analyzed during the current study are available from the corresponding author upon reasonable request.

Funding: This research received no external funding.

Institutional Review Board Statement: The study was conducted in accordance with the Declaration of Helsinki and approved by the appropriate Institutional Review Board.

References

1. Sheikh M, Roshandel G, McCormack V, Malekzadeh R. Current Status and Future Prospects for Esophageal Cancer. Cancers (Basel). 2023;15(3):765. 10.3390/cancers15030765.
2. Jiang W, Zhang B, Xu J, Xue L, Wang L. Current status and perspectives of esophageal cancer: a comprehensive review. Cancer Commun (Lond). 2025;45(3):281–331. 10.1002/cac2.12645.
3. Nagata Y, Yamamoto S, Kato K. Immune checkpoint inhibitors in esophageal cancer: Clinical development and perspectives. Hum Vaccin Immunother. 2022;18(6):2143177. 10.1080/21645515.2022.2143177.

4. Ouyang P, Wang L, Wu J, et al. Overcoming cold tumors: a combination strategy of immune checkpoint inhibitors. Front Immunol. 2024;15:1344272. 10.3389/fimmu.2024.1344272.
5. Lu Z, Zhang Q, Han J, Ji J, Xing X. Tumor microenvironment dynamics in gastric cancer pathogenesis and therapeutic resistance. Mol Cancer. 2026;25(1):58. 10.1186/s12943-026-02572-2.
6. Ton Nu QC, Park PH. Metabolic modulation of $CD8^+$ T cells by metformin: A promising adjuvant strategy for $CD8^+$ T Cell-Based Immunotherapies. Pharmacol Res. 2025;222:108015. 10.1016/j.phrs.2025.108015.
7. Xiao D, Zhang H, Liu Y, Li Y, Li G, Ning Y. Oncolytic viruses: advanced strategies in cancer therapy. Sig Transduct Target Ther. 2026;11(1):45. 10.1038/s41392-025-02343-3.
8. Sivanandam V, LaRocca CJ, Chen NG, Fong Y, Warner SG. Oncolytic Viruses and Immune Checkpoint Inhibition: The Best of Both Worlds. Mol Ther Oncolytics. 2019;13:93–106. 10.1016/j.omto.2019.04.003.
9. Ma R, Li Z, Chiocca EA, Caligiuri MA, Yu J. The emerging field of oncolytic virus-based cancer immunotherapy. Trends Cancer. 2023;9(2):122–39. 10.1016/j.trecan.2022.10.003.
10. Wang H, Borlongan M, Hemminki A, et al. Viral Vectors Expressing Interleukin 2 for Cancer Immunotherapy. Hum Gene Ther. 2023;34(17–18):878–95. 10.1089/hum.2023.099.
11. Downs-Canner S, Guo ZS, Ravindranathan R, et al. Phase 1 Study of Intravenous Oncolytic Poxvirus (vvDD) in Patients With Advanced Solid Cancers. Mol Ther. 2016;24(8):1492–501. 10.1038/mt.2016.101.
12. Park SH, Breitbach CJ, Lee J, et al. Phase 1b Trial of Biweekly Intravenous Pexa-Vec (JX-594), an Oncolytic and Immunotherapeutic Vaccinia Virus in Colorectal Cancer. Mol Ther. 2015;23(9):1532–40. 10.1038/mt.2015.109.
13. Evgin L, Acuna SA, Tanese de Souza C, et al. Complement Inhibition Prevents Oncolytic Vaccinia Virus Neutralization in Immune Humans and Cynomolgus Macaques. Mol Ther. 2015;23(6):1066–76. 10.1038/mt.2015.49.
14. Shen Z, Liu X, Fan G, et al. Improving the therapeutic efficacy of oncolytic viruses for cancer: targeting macrophages. J Transl Med. 2023;21:842. 10.1186/s12967-023-04709-z.
15. Liu Z, Ge Y, Wang H, et al. Modifying the cancer-immune set point using vaccinia virus expressing re-designed interleukin-2. Nat Commun. 2018;9:4682. 10.1038/s41467-018-06954-z.
16. Thorne SH, Hwang THH, O'Gorman WE, et al. Rational strain selection and engineering creates a broad-spectrum, systemically effective oncolytic poxvirus, JX-963. J Clin Invest. 2007;117(11):3350–8. 10.1172/JCI32727.
17. Gibson MK, Zaidi AH, Davison JM, et al. Prevention of Barrett Esophagus and Esophageal Adenocarcinoma by Smoothened Inhibitor in a Rat Model of Gastroesophageal Reflux Disease. Ann Surg. 2013;258(1):82. 10.1097/SLA.0b013e318270500d.
18. Kosovec JE, Zaidi AH, Komatsu Y, et al. Establishing magnetic resonance imaging as an accurate and reliable tool to diagnose and monitor esophageal cancer in a rat model. PLoS ONE.

2014;9(4):e93694. 10.1371/journal.pone.0093694.

19. Pyreddy S, Kim S, Miyamoto W, Talib Z, GnanaDev DA, Rahnemai-Azar AA. Current Advances in Immunotherapy Management of Esophageal Cancer. Cancers (Basel). 2025;17(5):851. 10.3390/cancers17050851.
20. Fayyad-Kazan M, Al-Tameemi S, Ouhtit A. Oncolytic Viruses in Cancer Immunotherapy: From Molecular Engineering to Clinical Translation. Cells. 2026;15(5):393. 10.3390/cells15050393.
21. Redelman-Sidi G, Glickman MS, Bochner BH. The mechanism of action of BCG therapy for bladder cancer–a current perspective. Nat Rev Urol. 2014;11(3):153–62. 10.1038/nrurol.2014.15.

Figures

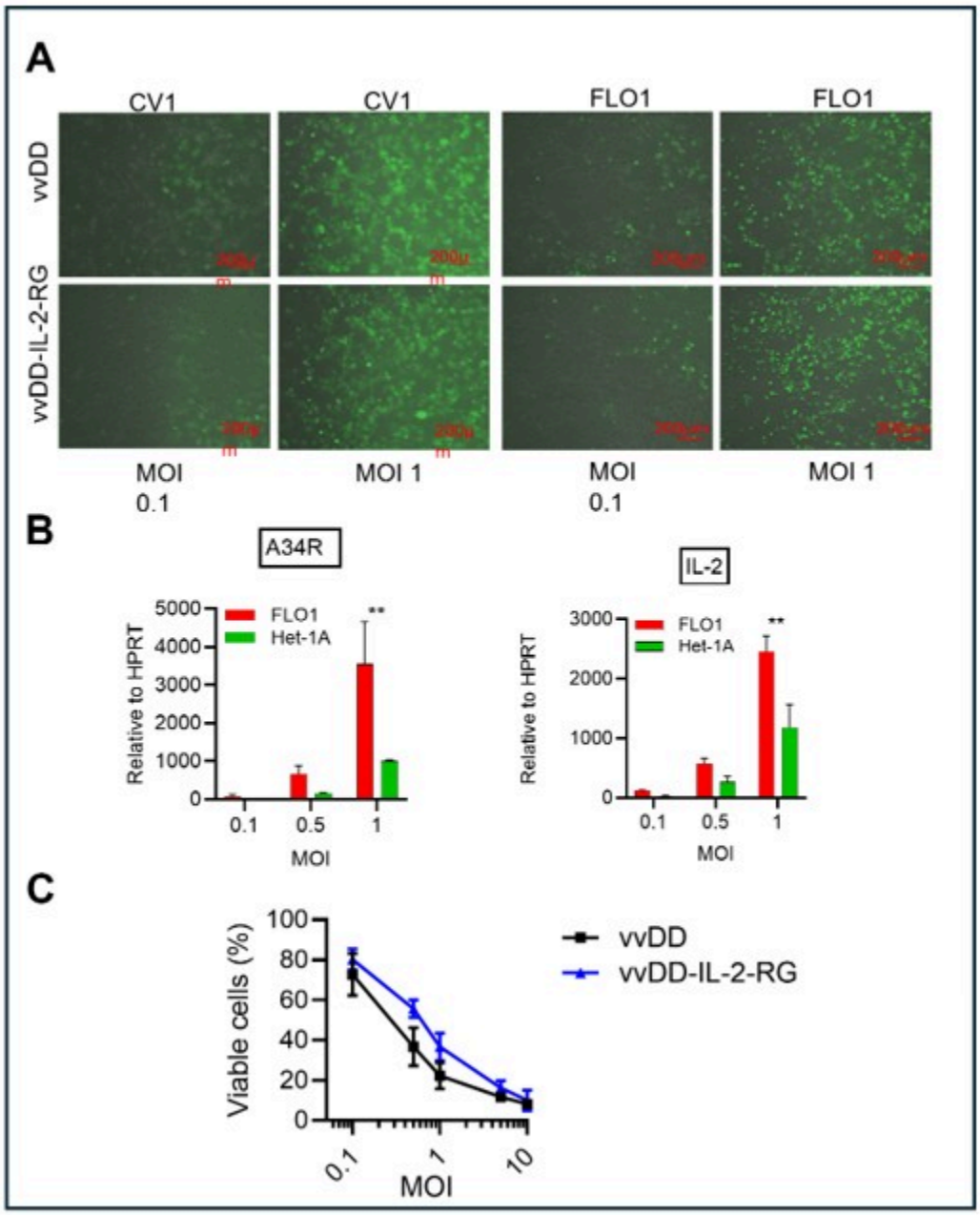


Figure 1

Engineering and validation of the IL-2–expressing oncolytic vaccinia virus (vvDD-IL-2-RG).(A) Infection of CV-1 fibroblasts and FLO-1 esophageal adenocarcinoma cells following exposure to vvDD or vvDD-IL-2-RG at indicated multiplicities of infection (MOIs), visualized by YFP fluorescence microscopy.(B) Quantitative RT-PCR analysis of viral replication in FLO-1 and Het-1A cells following infection with vvDD-IL-2-RG. Viral replication was assessed by expression of the vaccinia housekeeping gene A34R. (C) Cell viability assay showing dose-dependent cytotoxicity of vvDD and vvDD-IL-2-RG in FLO-1 cells. Expression of IL-2 does not impair viral cytolytic activity. Data show one representative experiment. ***P*<0.01

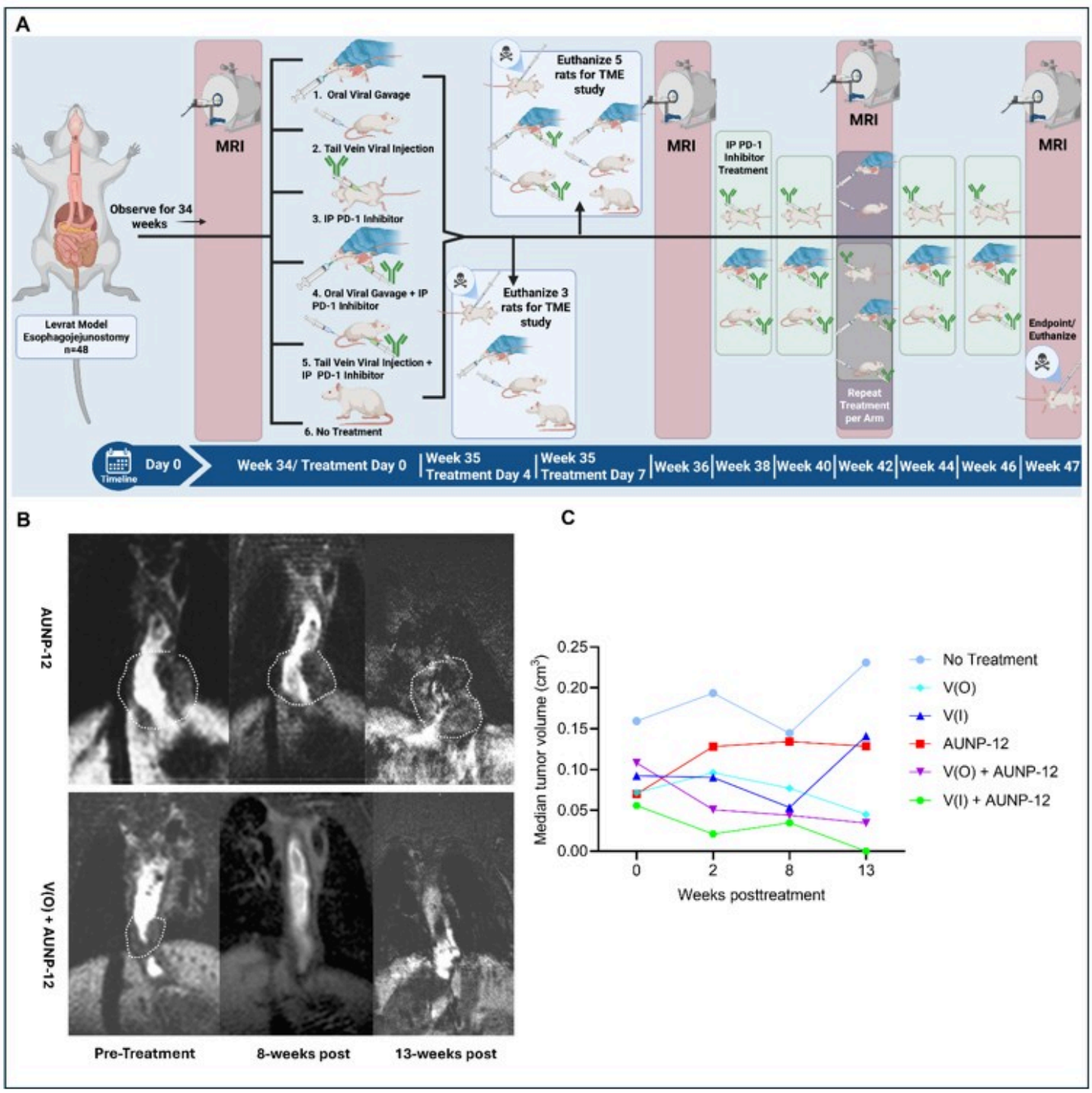


Figure 2

Experimental design and tumor response following viral therapy.
(A) Schematic overview of the treatment timeline in the modified Levrat EAC model. Animals were randomized to receive oral viral therapy, intravenous viral therapy, PD-1 inhibitor (AUNP-12), combination therapy, or no treatment. (B) Representative MRI images demonstrating tumor response across treatment groups. Tumors are indicated by arrows. **(C) Longitudinal MRI-based tumor volume measurements over time.** Data are presented as group medians with individual animal trajectories. Sample sizes (pre-treatment, 2 wk, 8 wk, 13 wk): V(I) n = 8, 7, 8, 6; V(O) n = 8, 9, 7, 4; AUNP-12 n = 7, 6, 6, 3; V(I) + AUNP-12 n = 5, 7, 6, 2; V(O) + AUNP-12 n = 8, 6, 6, 4; No treatment n = 2, 2, 2, 2. Linear mixed-effects model (likelihood ratio tests): time p = 0.014; treatment group p = 0.234; group × time interaction p = 0.419. Kruskal-Wallis tests at individual time points were non-significant (p = 0.094–0.659). See Methods for model specification.

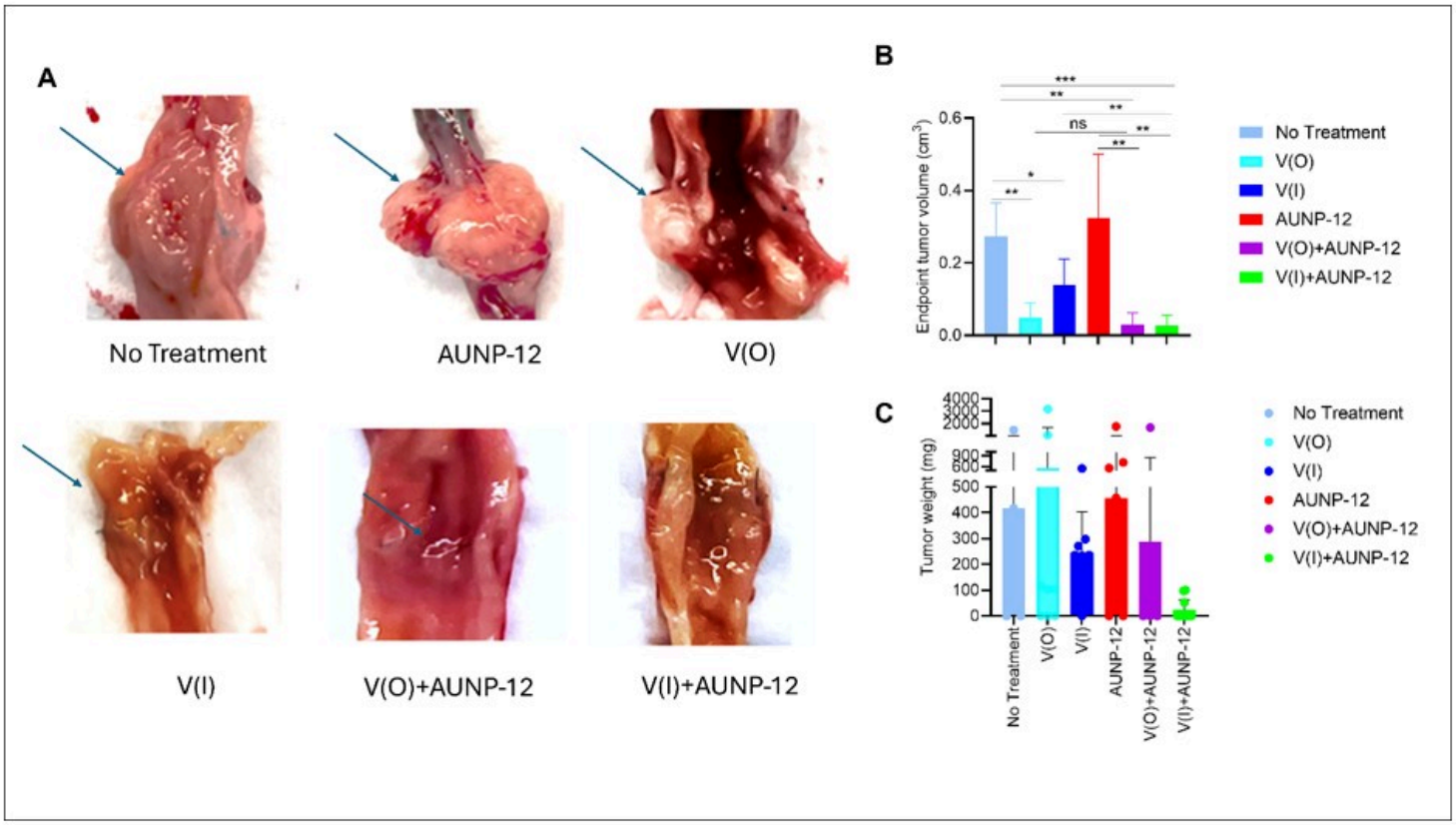


Figure 3

Gross Assessment of Esophageal Cancer Response to Treatment. An MRI was obtained to confirm the presence of an esophageal tumor. The rats were then divided into 6 groups (3-7 rats/group): 1) No treatment; 2) V(O); 3) V(I); 4) AUNP-12; 5) V(O) + AUNP-12; 6) V(I) + AUNP-12. The rats were observed after treatment for 13 weeks and then euthanized. The esophagus and tumor were excised from each animal. Photographs of representative tumors are shown (arrows denote palpable tumor) (**A).** The tumors were measured with calipers (**B**) and weighed Sample sizes (intent-to-treat, all necropsied

animals): V(I) n = 7; V(O) n = 8; AUNP-12 n = 8; V(I) + AUNP-12 n = 10; V(O) + AUNP-12 n = 7; No treatment n = 4. Kruskal-Wallis test: H = 10.12, p = 0.072. Pre-specified Mann-Whitney U tests with Benjamini-Hochberg correction. See Methods for statistical details. *P<0.05.

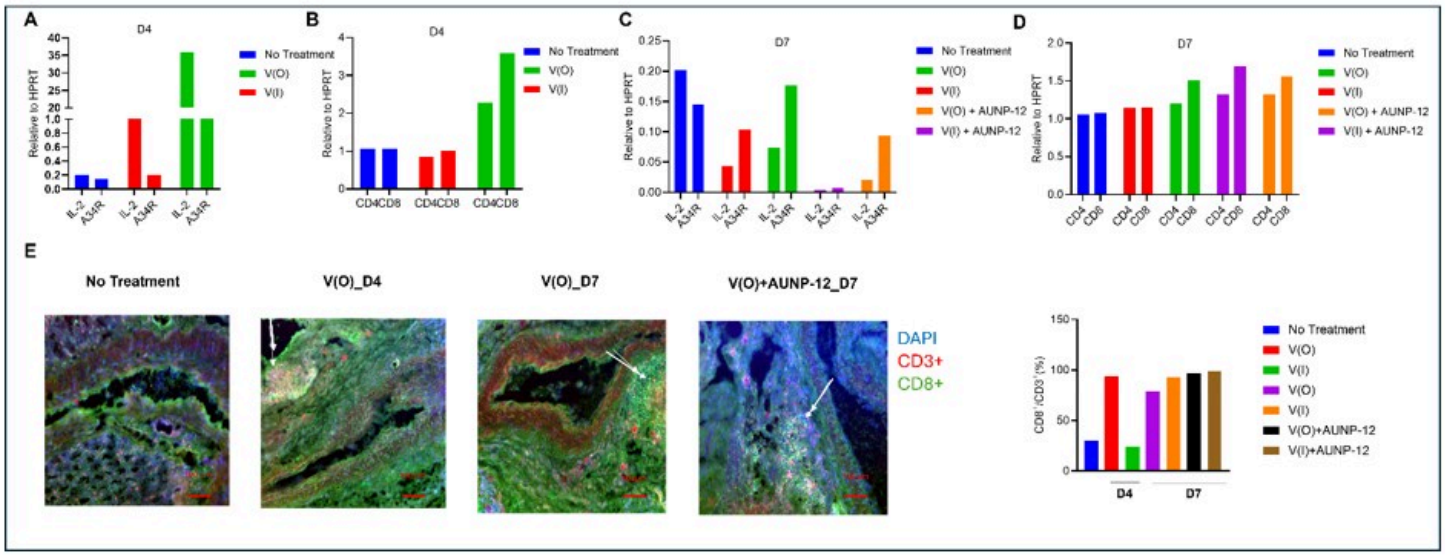


Figure 4

(A-D) Relative Gene Expression by RT-qPCR: Relative gene expression levels, normalized to HPRT, were measured for IL-2, A34R (viral gene), CD4, and CD8.(A) Day 4 (IL-2 and A34R): Shows IL-2 and A34R expression on Day 4. (B) Day 4 (CD4 and CD8): Displays CD4 and CD8 expression on Day 4. (C) Day 7 (IL-2 and A34R): Presents IL-2 and A34R expression on Day 7. IL-2 levels appear to normalize across all groups.(D) Day 7 (CD4 and CD8): Illustrates CD4 and CD8 expression on Day 7. (E) Immunofluorescence Staining and Quantification of CD8+/CD3+ Cells: Representative immunofluorescence images (left panels) display DAPI (blue, nuclei), CD3+ (red, pan T-cells), and CD8+ (green, cytotoxic T-cells) staining. White arrows highlight areas of immune cell infiltration. The adjacent bar graph (right panel) quantifies the percentage of CD8+ cells among total CD3+ cells (CD8+/CD3+) at Day 4 and Day 7 across different treatment groups. This panel visually supports the gene expression data, demonstrating varying levels of CD8+ T-cell infiltration.

Supplementary Files

This is a list of supplementary files associated with this preprint. Click to download.

- GA.jpg